IOP Publishing Journal of Physics B: Atomic, Molecular and Optical Physics
J. Phys. B: At. Mol. Opt. Phys. **50** (2017) 224001 (8pp) https://doi.org/10.1088/1361-6455/aa900c

Signatures and mechanisms of plasmon-enhanced electron emission from clusters in few-cycle laser fields

Lennart Seiffert[1], Jörg Köhn[1], Christian Peltz[1], Matthias F Kling[2,3] and Thomas Fennel[1,4]

[1] Institute of Physics, University of Rostock, Albert-Einstein-Straße 23, D-18059 Rostock, Germany
[2] Max Planck Institute of Quantum Optics, Hans-Kopfermann-Straße 1, D-85748 Garching, Germany
[3] Department of Physics, Ludwig-Maximilians-Universität München, Am Coulombwall 1, D-85748 Garching, Germany
[4] Max-Born-Institut, Max-Born-Straße 2A, D-12489 Berlin, Germany

E-mail: thomas.fennel@uni-rostock.de

Received 11 August 2017, revised 22 September 2017
Accepted for publication 29 September 2017
Published 30 October 2017

Abstract

Intense laser pulses with well-defined waveforms enable unprecedented control over electronic strong-field processes in atoms, molecules and nanostructures. In particular, carrier-envelope phase (CEP) controlled few-cycle pulses allow the modification of various features in high-harmonic or photoelectron spectra. Vice versa, such signatures open up the opportunity to identify the underlying physical processes. Here, we utilize this approach to investigate plasmon-enhanced electron emission from simple metal clusters under resonant few-cycle laser pulses. Photoelectron energy spectra extracted from our semiclassical trajectory simulations reveal a set of pronounced but strongly intertwined CEP-dependent signatures. We find, that electron trajectories associated with these signatures can be categorized by two characteristic timestamps, i.e. the escape from the cluster and the last transit through its central plane. A correlation analysis of these times enables us to disentangle the intertwined features and to associate them with different acceleration mechanisms. We expect that our results will support the interpretation of specific patterns in the photoelectron spectra of future CEP-resolved cluster experiments.

Keywords: waveform control, strong-field ionization, resonant excitation, few-cycle pulses, carrier-envelope phase, metal cluster, plasmon-enhanced electron emission

1. Introduction

The availability of laser pulses with well-defined electric field waveforms has opened systematic routes to control electronic processes in atoms, molecules, and nanostructures on the attosecond time scale [1–3]. For example, the active modification of the strong-field driven recollision dynamics of photoemitted electrons by the carrier-envelope phase of intense few-cycle laser pulses or via bichromatic laser fields enables control over the resulting high-harmonic emission [4–7] and electron energy spectra [8–13]. In fact, the modification of such spectra via the field waveform does not only reflect powerful control but also provides a useful fingerprint for the identification of the underlying physics. Recent examples that exploit this strategy include the analysis of the sub-cycle evolution of atomic tunneling [6] and the near-field enhanced photoemission from nanotips [7, 11] and isolated nanoparticles [10, 14–16]. In the latter two cases, CEP-dependent signatures in the photoelectron spectra unambiguously showed the dominance of elastic backscattering in the high energy photoemission.

The generation of particularly energetic electrons can be expected from an acceleration in a resonantly enhanced near-field of a plasmonic nanostructure. Such scenario is realized in the plasmon-enhanced electron emission from clusters, where a transient resonance state is prepared by preionization and subsequent expansion of the cluster. This preparation can take place in the leading pulse edge [17] or can be initiated by

an additional preceding activation pulse [18]. It should further be noted that resonant excitation without the need of preceding expansion has been demonstrated for rare-gas doped helium droplets under near-infrared few-cycle pulses [19]. Previous theoretical studies support that single-cycle forward rescattering dominates the high energy electron emission in the case of clusters [20, 21] and leads to the observed particularly strong enhancement of laser aligned emission of fast electrons [22, 23]. However, in experiments, a complete characterization of all relevant processes contributing to the electron emission has been difficult with so far employed long pulses, as electron spectra alone contain insufficient information for such discrimination.

The goal of the current theoretical study is to explore which phase-dependent signatures could be expected from an experiment on clusters with resonant few-cycle excitation to achieve detailed insight into the underlying mechanisms. Our analysis addresses at least three important fundamental aspects. First, it is so far unclear if and to which extent plasmonic resonance enhancement in the electron emission is operational with extremely short pulses in the few-cycle regime. Second, the shape and possible significance of CEP-dependent features in the spectra of a few-cycle cluster experiment are unknown. Their clarification could justify corresponding experimental investigations. Third, the potentially relevant mechanisms and their connection to phase-dependent spectral patterns are unclear. In conclusion, a systematic qualitative characterization of the few-cycle response and the connection of processes with experimentally accessible observables is desirable.

In order to tackle the questions above we consider small jellium spheres as a representative model for simple metal clusters and model their resonant few-cycle response with semiclassical Thomas–Fermi–Vlasov molecular dynamics simulations [24, 25]. As our central goal is a systematic and transparent analysis of the qualitative features of the few-cycle driven resonant photoemission, we further neglect electron–electron collisions in our exploratory study. We analyze the CEP-dependence of angular-resolved photoelectron energy spectra and develop a correlation map analysis that enables the efficient classification of trajectories and allows their association with individual emission processes. Using this method we disentangle the features from direct emission, forward-rescattering, and large-angle emission in the electron spectra and isolate their specific signatures that could be expected in experiments. In theory, a CEP-resolved correlation map analysis further allows the distinction of sub-cycle contributions for the individual processes. Our results strongly support that significant features could be expected in experiments and that different emission processes could be identified via their specific signatures in the CEP-dependent spectra.

The remainder of the manuscript is structured as follows. In section 2 we briefly summarize the elements of the semiclassical simulation method and discuss the parameters of our analysis. The presentation of the results in section 3 is divided as follows. First, in section 3.1 we discuss a typical simulation run in detail and present angular and energy-resolved electron spectra. In section 3.2 we inspect characteristic trajectories to motivate our correlation map analysis that is discussed in section 3.3. Utilizing this analysis in section 3.4, we present the mechanism-specific emission spectra followed by a discussion of the sub-cycle resolved contributions in section 3.5. Finally, we summarize our results in section 4.

2. Methods

To describe the laser-driven valence electron dynamics in the clusters we employ the semiclassical Thomas–Fermi–Vlasov molecular dynamics method. The semiclassical description can be derived from time-dependent density-functional theory and was used successfully to describe laser-cluster excitation [21, 24, 26]. For clarity, we focus on the collective dynamics in our current analysis. We therefore neglect electron–electron collisions and the detailed atomic structure by describing the ionic background in jellium approximation [27, 28]. Previous studies for similar parameter regimes showed that including electron–ion and electron–electron collisions does affect the plasmon lifetime and the details of the photoelectron distribution, but leaves the qualitative picture of the ionization dynamics unchanged [29–31]. The detailed study of collisional effects on the few-cycle dynamics is therefore postponed to a later quantitative analysis. To prepare a resonant plasmonic state the density n_i of the ionic jellium background is chosen according to the resonance density of the classical Mie-plasmon

$$\omega = \sqrt{\frac{e^2 n_\mathrm{i}}{3\varepsilon_0 m}},$$

where ω is the angular frequency of the driving laser field, e the elementary charge, m the electron mass and ε_0 the vacuum permittivity. The technical aspects of the method are described in detail elsewhere [24]. In brief, the one-body phase-space distribution of the electrons $f(\mathbf{r}, \mathbf{p}, t)$ is initialized with the Fermi–Dirac distribution at temperature $T = 0$ and propagated self-consistently according to the Vlasov equation

$$\left[\frac{\partial}{\partial t} + \frac{\mathbf{p}}{m}\nabla_r - V_\mathrm{eff}(\mathbf{r}, t)\overleftarrow{\nabla_r}\cdot\vec{\nabla}_p\right] f = 0.$$

The effective potential for the electrons

$$V_\mathrm{eff} = V_\mathrm{ion} + V_\mathrm{ee}[n_\mathrm{e}] + V_\mathrm{xc}[n_\mathrm{e}] + V_\mathrm{ext}$$

contains the ionic jellium background V_ion, the Hartree potential $V_\mathrm{ee}[n_\mathrm{e}]$ and the exchange-correlation potential $V_\mathrm{xc}[n_\mathrm{e}]$. The external potential $V_\mathrm{ext} = ez\mathcal{E}(t)$ describes the excitation by the laser $\mathcal{E}(t) = \mathcal{E}_0(t)\cos(\omega t + \varphi_\mathrm{CE})$ that is polarized in z-direction and has a Gaussian envelope $\mathcal{E}_0(t)$ and carrier-envelope phase φ_CE. Note that the Hartree and exchange-correlation potentials depend self-consistently on the electron density $n_\mathrm{e}(\mathbf{r}, t) = \int f(\mathbf{r}, \mathbf{p}, t)\mathrm{d}^3p$. The Hartree potential is calculated using a parallel multigrid solver and for the exchange-correlation potential we employ the local density approximation [26] as parametrized in [32]. The actual dynamics is solved with a pseudo-particle method using the same parameters as in [24].

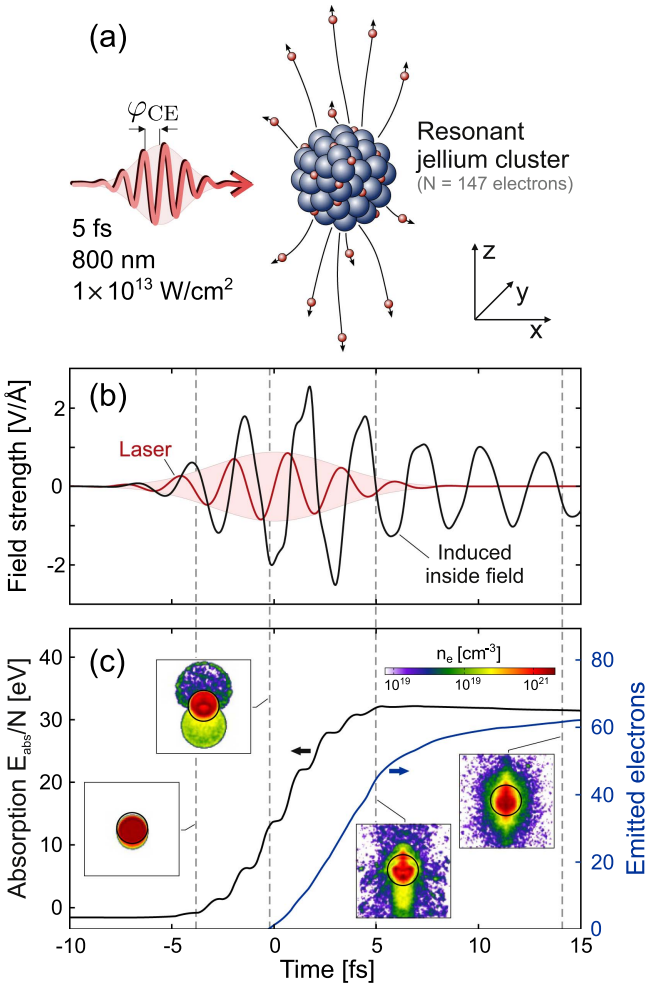

Figure 1. Ionization dynamics of a jellium cluster under resonant excitation with a near-infrared few-cycle pulse. (a) Schematic representation of the reference scenario. (b) Field-strength of the incident laser (red) with $\varphi_{CE} = 1.5\pi$ and of the induced field inside the cluster (black). (c) Energy absorption per atom (black) and number of emitted electrons (blue). Insets show the transient electron density in the polarization-propagation plane for selected moments (vertical dashed lines) during the ionization process. Black circles indicate the jellium background radius $R = 18.9$ Å.

3. Results and discussion

3.1. Reference scenario

In the current study we consider small jellium spheres ($N = 147$ electrons) as a representative model for simple metal clusters with nearly free conduction electrons. The clusters are excited by 5 fs (intensity FWHM) laser pulses at 800 nm wavelength with intensity $I = 1 \times 10^{13}$ W cm^{-2}. The plasmon resonance is realized by pre-expansion of the cluster to a density of $n_i = 5.2 \times 10^{21}$ cm^{-3}. A schematic setup of the scenario is shown in figure 1(a). Selected global observables for a typical run are displayed in figures 1(b), (c). The comparison of the electric field induced inside the cluster to the incident laser field in figure 1(b) reveals clear signatures of strong resonance enhancement. The amplitude of the induced field substantially exceeds that of the laser field and exhibits a phase lag of approximately $\pi/2$. Additional evidence for the resonant excitation of the eigenfrequency of the collective dipole mode is given by the ringing of the induced field after the laser pulse. A clear signature for nonlinear excitation is the presence of higher frequency components as reflected by the anharmonic shape of the induced field. Note that the lifetime of the induced plasmon oscillation is overestimated when neglecting electron–electron collisions [29–31]. However, the resulting effect on the electron emission spectra is expected to be small as the dominant contribution of electrons is emitted during the laser pulse (see figure 1(c)). As a result of the resonant excitation the cluster absorbs a substantial amount of energy (around 30 eV per atom, black curve in figure 1(c)) and emits almost half of the valence electrons (blue curve in figure 1(c)). The snapshots of the transient electron density in the propagation-polarization plane (insets in figure 1(c)) reveal sub-cycle bursts of electrons with preferential emission along the laser polarization axis.

In order to explore the CEP-dependence we performed a set of simulations by scanning the CEP in the range $\varphi_{CE} = 0$ to 2π in steps of 0.05π. The global features of the electron emission are presented in the CEP-averaged angular and energy-resolved electron spectrum in figure 2(a). The data shows clear enhancement of the emission along the laser polarization direction and a global shape of the spectrum similar to previous results obtained for resonant excitation with long pulses [21, 23]. We like to briefly discuss the magnitude of the observed electron cutoff energy of about 100 eV. The natural energy scale connected to the forward rescattering process results from the picture of a half-cycle transit. The kinetic energy E_{hct} of an impinging electron associated with the resulting average velocity $v_{hct} = 2R/(T/2)$, where R is the cluster radius and T is the period of the driving field, dictates the energy scaling with cluster size and wavelength. Of course, also the intensity has to be sufficiently high to drive the plasmonic process. For our example ($R = 18.9$ Å, $\lambda = 800$ nm), this energy scale is $E_{hct} = 23$ eV. The fact that the actual cutoff energy is higher shows that the few-cycle scenario differs from the simple ballistic half-cycle transit picture. Considering the same average velocity and the fact that energetic electrons are accelerated in a single half-cycle starting at rest (see red trajectory in figure 3(b)) leads to a final velocity of $v_{final} = 2v_{hct}$. The resulting energy ($E_{final} = 4E_{hct} \approx 100$ eV) is in reasonable agreement with our data. Despite the similar overall shape, compared to previous results in the long pulse regime the spectrum in this study is much more structured and contains sharp features marked with labels 1–4. These structures hint at the presence of contributions from qualitatively different emission processes.

In order to compare the phase-dependencies of these contributions, figure 2(b) displays the evolution of the upward and downward emission (see red sectors in figure 2(a)). The spectrum reveals distinct CEP-dependent features, demonstrating the feasibility of waveform control. While feature 1 corresponds to relatively slow electrons and exhibits an arch-like structure, features 2 and 3 show a finger-like shape extending to high energies. Note that feature 4 in figure 2(a)

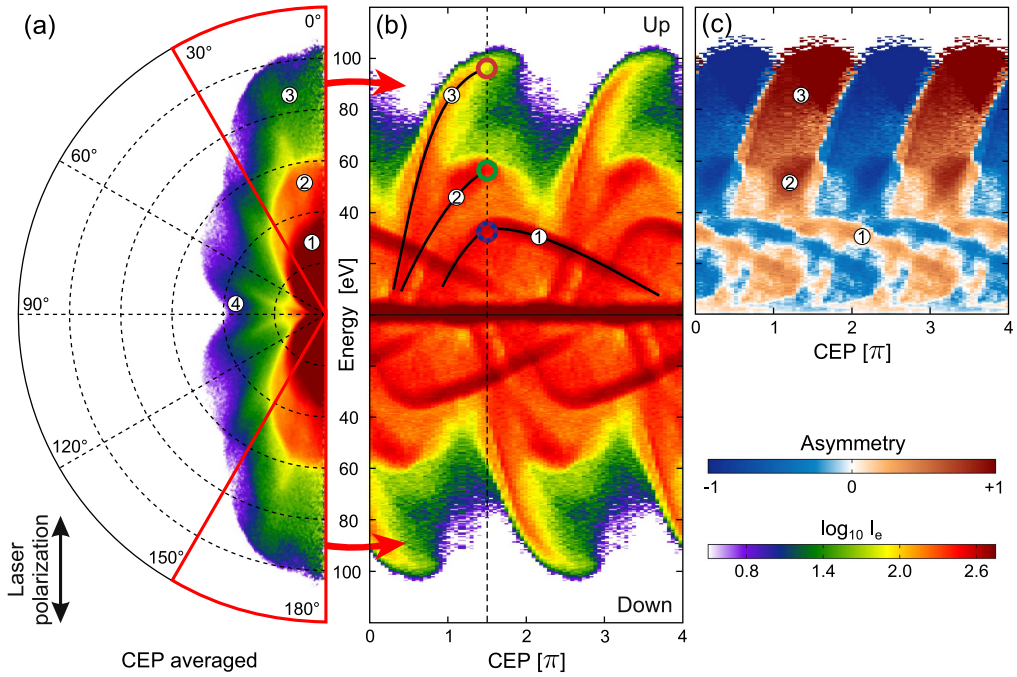

Figure 2. Energy spectra of electrons emitted from a resonantly driven jellium cluster ($N = 147$). Labels 1–4 indicate the most prominent spectral features. (a) CEP-averaged angle-resolved energy spectrum $I_e(E, \theta)$ including all electrons emitted under angles θ with respect to the laser polarization axis. (b) Phase-dependent electron emission in upward $I_e^u(E, \varphi_{CE})$ and downward $I_e^d(E, \varphi_{CE})$ direction (integrated within an angle of 30 ° with respect to the laser polarization axis, see red frames in (a)). Black curves visualize the CEP-dependence of the three dominant signatures. Colored circles at $\varphi_{CE} = 1.5\pi$ (vertical dashed line) indicate the final energies of selected trajectories analyzed in figure 3. (c) Map of the CEP-dependent up–down asymmetry $A(E, \varphi_{CE}) = \frac{I^u - I^d}{I^u + I^d}$, where stronger upward/downward emission is visualized as red/blue.

represents electrons emitted under large angles with respect to the laser polarization axis and therefore does not appear in the upward and downward emission spectra. An alternative visualization of the phase-dependence is offered by up–down emission-asymmetry maps, as often used in experimental studies. The asymmetry map in figure 2(c) reveals a left-tilted pattern at lower energies that can be attributed to the arch-like feature 1 and right-tilted contributions at higher energies, that are connected to features 2 and 3. These opposing trends strongly indicate the dominance of different acceleration mechanisms in the specific energy ranges. However, their further characterization based on the CEP-dependent spectra or the asymmetry maps alone remains difficult.

3.2. Trajectory analysis

In the following we develop a filter method that enables the discrimination of the different process-specific spectral contributions based on electron trajectories. Therefore, we first motivate which aspects of the trajectories are useful for such filtering. To this end, we analyze four representative groups of trajectories contributing to the pronounced features in the CEP-dependent data (see colored circles in figure 2(b)). For each group the evolution of an averaged trajectory is depicted in figure 3(b). The following group-specific signatures can be observed in the averaged trajectories. The group 1 trajectory (blue) exhibits a quiver motion in the upper half of the cluster followed by upward emission. In what follows we associate trajectories with long residence times (more than a half-cylce) within the emission half-space with a direct emission process. In contrast, the representative trajectories for the other three groups cross the cluster center shortly before the emission, reflecting forward-rescattering processes. Among these groups, group 2 (green) and group 3 (red) trajectories undergo a full passage through the cluster with a turning point near the cluster edge and are therefore termed full forward rescattering. The group 1a trajectory (purple) exhibits a turning point near the cluster center, resembling only partial forward rescattering. In fact, full forward rescattering leads to the highest final energies, while direct emission and partial forward rescattering result in lower energies, see evolution of the respective single particle energies in figure 3(c). Furthermore, full forward rescattering is characterized by two phases of strong energy gain before and after the passage through the cluster center (solid green and red curves). In contrast, partial forward rescattering and direct emission correspond to only a single strong gain period (solid purple and blue curves). Note that for all trajectories the energy gain from the polarization field is dominant, i.e. larger than the gain from the driving laser field (compare dark versus light bars on the right of figure 3(c)).

The group-specific features of the different trajectories motivate a trajectory discrimination based on two representative timestamps, i.e. the last transit through the cluster center (t_{trans}, defined by the passage through the $z = 0$ plane) and the escape from the cluster volume (t_{esc}, defined by the

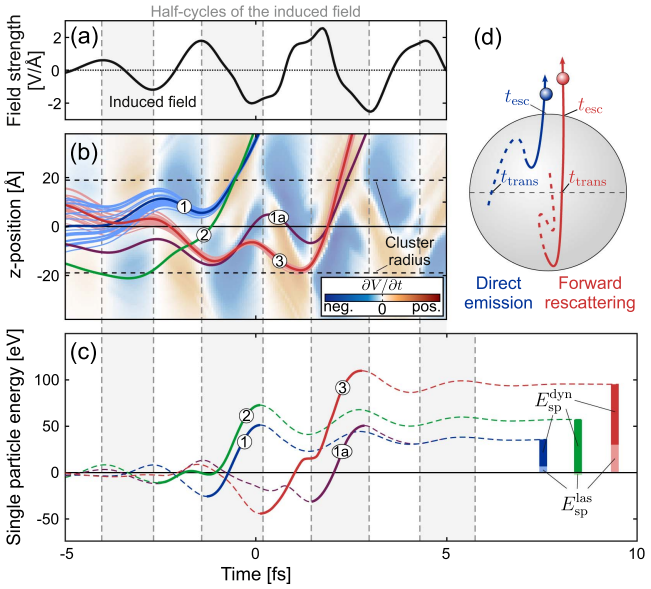

Figure 3. (a) Time-evolution of the induced field inside the cluster. Vertical dashed lines and gray shaded areas indicate the half-cycles. (b) Representative trajectories (dark) averaged within four groups (labeled as 1, 1a, 2 and 3) of electrons with asymptotic energies indicated by the respectively colored circles in figure 2(b). Note that trajectories in groups 1 and 1a result in similar final energies and are therefore distinguished by the respective emission cycles. For groups 1 and 3 full ensembles of trajectories are shown as light curves to illustrate the trajectory averaging. The background depicts the local rate of change of the cluster potential on the polarization axis z, indicating energy gain/loss from the plasmonic field in red/blue regions. (c) Single particle energy E_{sp} of the averaged trajectories (dashed). The solid sections of the curves highlight the pivotal time intervals with dominant energy gains. Bars on the right indicate selective energy gains from the laser field $E_{\mathrm{sp}}^{\mathrm{las}}$ and the plasmonic field $E_{\mathrm{sp}}^{\mathrm{dyn}}$ calculated via a selective analysis of the single particle energy gain rate $\dot{E}_{\mathrm{sp}} = -e\mathbf{E}_{\mathrm{las}} \cdot \dot{\mathbf{r}} + \frac{\partial}{\partial t} V(\mathbf{r}, t)$ [33]. The first term $\dot{E}_{\mathrm{sp}}^{\mathrm{las}} = -e\mathbf{E}_{\mathrm{las}} \cdot \dot{\mathbf{r}}$ describes the energy gain from the laser field in the presence of a static potential (see [20]) and the second term represents energy gain from the plasmonic field $\dot{E}_{\mathrm{sp}}^{\mathrm{dyn}} = \frac{\partial}{\partial t} V(\mathbf{r}, t)$. (d) Schematic representation of trajectories before (dashed) and during (solid) the emission half-cycle for direct emission (blue) and forward rescattering (red) and the corresponding times of the last transit through the central plane t_{trans} and escape from the cluster t_{esc}.

passage through the jellium sphere surface). In particular, the difference of these timestamps can be used to distinguish direct emission from forward rescattering, see figure 3(d). Note that for direct emission the last transit takes place before the emission half-cycle. Furthermore, directly emitted electrons that start in the upper half-sphere might not cross the symmetry plane at all.

3.3. Correlation map analysis

The distribution of transit and escape times of all trajectories contributing to the spectrum in figure 2(a) (including all CEPs) is shown in the correlation map in figure 4 and reveals clearly separated features. We assign these features to the different emission mechanisms that are visualized by the four sketches. The first feature (blue frame) represents trajectories with escape

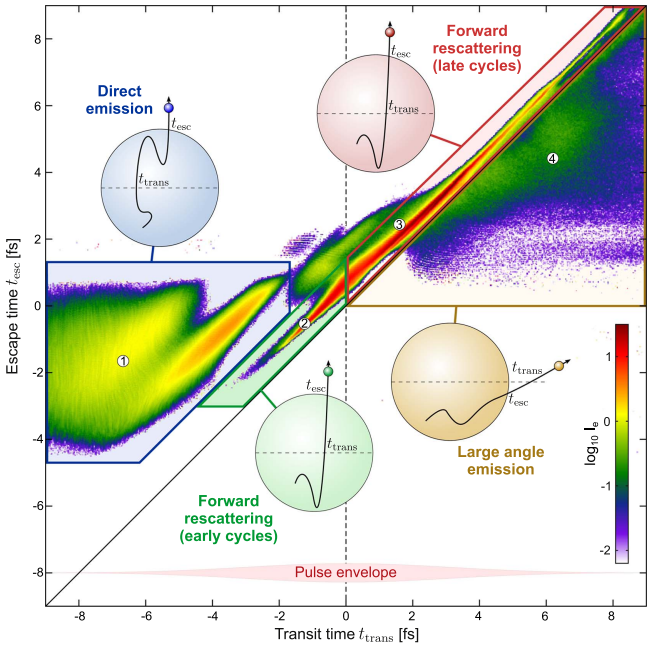

Figure 4. CEP-averaged correlation map of the transit times t_{trans} and escape times t_{esc} of all electrons contributing to the spectrum in figure 2(a). Colored areas mark the signatures corresponding to four different classes of trajectories illustrated by the respective sketches (see figure 3(d)). The diagonal line indicates $t_{\mathrm{trans}} = t_{\mathrm{esc}}$. The vertical dashed line indicates the center of the laser pulse (see envelope at the bottom). Labels 1–4 indicate the connection of the features in the correlation map with the trajectories in figure 3 and the spectral signatures in figures 2 and 5.

times more than a half-cycle after the last transit and is therefore associated with the direct emission process. Second, the feature below the diagonal (yellow frame) corresponds to electrons that cross the central plane after being emitted from the cluster, i.e. $t_{\mathrm{trans}} > t_{\mathrm{esc}}$. The respective sketch indicates that this condition is typically met by electrons emitted under large angles with respect to the laser polarization axis. The third signature is aligned parallel and near to the diagonal ($t_{\mathrm{esc}} > t_{\mathrm{trans}}$), indicating a strong correlation of transit and escape times. This signature corresponds to forward rescattered electrons and its vicinity to the diagonal indicates a rapid transit through the cluster. We further distinguish between electrons passing the central plane before and after the maximum of the laser field envelope to separate forward rescattering in the early cycles (green frame) and late cycles (red frame).

3.4. Selective energy spectra

Based on the above classification of the trajectories via the correlation map we are now able to calculate selective energy spectra for electrons emitted via the different acceleration mechanisms, see figure 5. These spectra reveal a distinct separation of the signatures contributing to the full spectra shown in figure 2 that can now be unambiguously assigned to the different mechanisms. Direct emission (figures 5(a)–(c)) results in a dipole-like shape in the angle-resolved energy spectrum and creates the arch-shaped low energy features in the CEP-dependent spectrum that correspond to asymmetries tilted

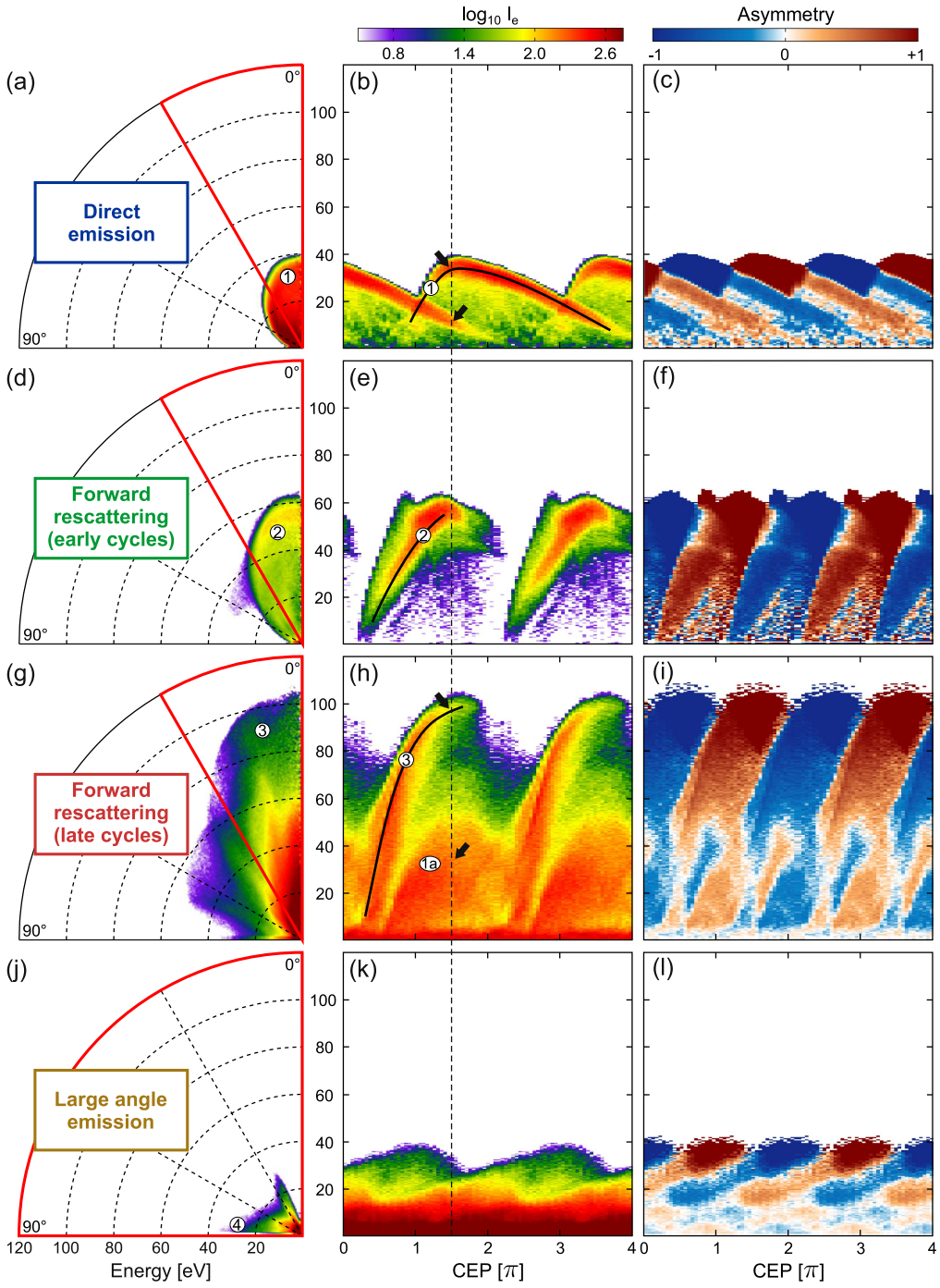

Figure 5. Selective spectra of directly emitted electrons (a)–(c), electrons emitted after forward rescattering in the early cycles of the laser field (d)–(i) and the later cycles (g)–(f), and electrons emitted under large angles with respect to the laser polarization direction (j)–(l). Note that the CEP-dependent electron spectrum (k) and the respective asymmetry map (l) for emission under large angles are obtained via integration over emission angles up to 90°, see red frame in (j).

to the left. Forward rescattering in the early cycles (figures 5(d)–(f)) and late cycles (figures 5(g)–(i)) forms the higher energy contributions and is directly connected with the finger-shaped signatures in the CEP-resolved spectra and right-tilted asymmetries. The fourth class of selective spectra (figures 5(j)–(l)) indicates, that electron emission at large angles exhibits a phase-dependence similar to forward rescattering but results in significantly lower energies. In particular, for direct emission and forward rescattering in the early cycles we could identify very sharp and distinct signatures. However, the spectra of forward rescattering in the late cycles still seem to contain two different contributions whose underlying mechanisms could not be resolved in the CEP-averaged correlation map.

3.5. CEP-resolved correlation map

The identification of the mechanisms resulting in the two spectral contributions in figure 5(h) can be achieved by the

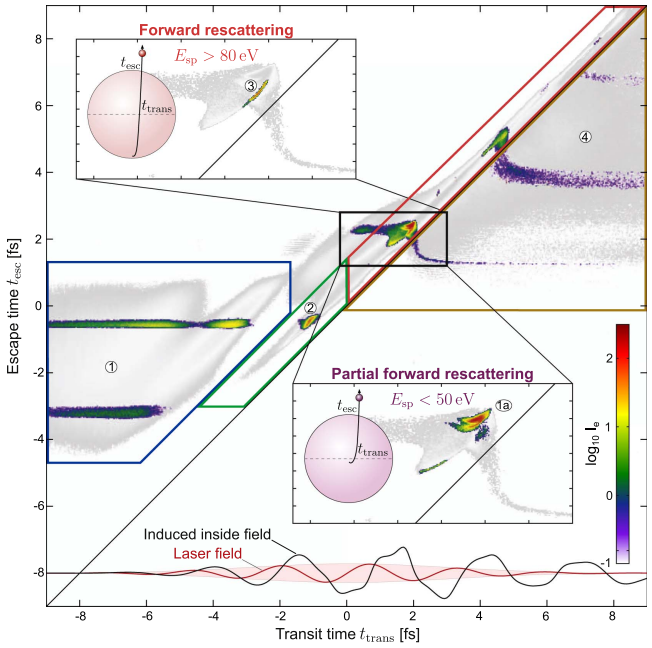

Figure 6. CEP-resolved correlation map ($\varphi_{CE} = 1.5\pi$) of electrons emitted in upward direction. The grayscale image in the background visualizes the CEP-averaged full correlation map, see figure 4. Insets show a magnification of the dominant feature for forward rescattering in the late cycles (black rectangle) in grayscale. The colored spectra within the insets show selective correlation maps for electrons emitted in polarization direction (30° opening angle) and with high (top inset) and low (bottom inset) final energies (as indicated). The sketches visualize the respective full and partial forward-rescattering mechanisms (see figure 3(d)).

inspection of a CEP-resolved correlation map for $\varphi_{CE} = 1.5\pi$ where both contributions are present in the energy spectrum (see dashed line and black arrows in figure 5(h)). Such a map (see figure 6) enables to resolve the sub-cycle evolution of the emission. For example, it exhibits two well separated features for direct emission in subsequent cycles (blue frame) corresponding to the two signatures in the respective spectrum (black arrows in figure 5(b)). Furthermore, the features corresponding to forward rescattering in the early cycles (green frame) and late cycles (red frame) are now clearly separated. Note that for the latter process only one cycle (black rectangle) contributes significantly to the electron spectra and includes trajectories corresponding to both features in figure 5(h). As a further separation of this dominant feature in the correlation map is impossible via the transit and escape times only we apply an additional filter based on the final electron energies. This selective analysis reveals that electrons with high final energies (>80 eV, top inset) correspond to a very sharp feature parallel and close to the diagonal in the CEP-resolved correlation map. Analysis of the respective trajectories indicates that these electrons where accelerated by full forward rescattering (see red trajectories in figure 3(b)). In contrast, electrons with low final energies (<50 eV, bottom inset) can be associated with partial forward rescattering and result in a broadened feature in the correlation map further away from the diagonal (see purple trajectories in figure 3(b)).

4. Conclusion

In summary, we investigated plasmon-enhanced electron emission from clusters in intense few-cycle laser fields and studied the resulting carrier-envelope phase-dependent emission spectra. We found clear resonance enhancement and distinct CEP-dependent features in the angle and energy-resolved electron spectra. Our correlation map analysis of the trajectories enabled an efficient separation of the contributing acceleration mechanisms and the separation of their signatures in the spectra. Knowledge of the specific patterns in the CEP-dependent spectra and asymmetry maps are expected to guide the interpretation of future CEP-resolved cluster experiments. Furthermore, the basic concept of the correlation map analysis is expected to be applicable to various other scenarios.

Acknowledgments

LS, CP and TF gratefully acknowledge financial support from the Deutsche Forschungsgemeinschaft within SFB 652/3 and computer time provided by the North-German Supercomputing Alliance HLRN (project ID mvp00011). MFK is grateful for support by the European Union via the ERC grant ATTOCO (no. 307203).

ORCID iDs

Lennart Seiffert https://orcid.org/0000-0002-2389-5295
Matthias F Kling https://orcid.org/0000-0002-1710-0775
Thomas Fennel https://orcid.org/0000-0002-4149-5164

References

[1] Krausz F and Ivanov M 2009 *Rev. Mod. Phys.* **81** 163–234
[2] Wollenhaupt M and Baumert T 2011 *Faraday Discuss.* **153** 9–26
[3] Ciappina M F *et al* 2017 *Rep. Prog. Phys.* **80** 054401
[4] Dudovich N, Smirnova O, Levesque J, Mairesse Y, Ivanov M Y, Villeneuve D M and Corkum P B 2006 *Nat. Phys.* **2** 781–6
[5] Goulielmakis E *et al* 2008 *Science* **320** 1614–7
[6] Shafir D, Soifer H, Bruner B D, Dagan M, Mairesse Y, Patchkovskii S, Ivanov M Y, Smirnova O and Dudovich N 2012 *Nature* **485** 343–6
[7] Ott C *et al* 2013 *New J. Phys.* **15** 073031
[8] Paulus G G, Lindner F, Walther H, Baltuška A, Goulielmakis E, Lezius M and Krausz F 2003 *Phys. Rev. Lett.* **91** 253004
[9] Kling M F, Rauschenberger J, Verhoef A J, Hasović E, Uphues T, Milošević D B, Muller H G and Vrakking M J J 2008 *New J. Phys.* **10** 025024
[10] Zherebtsov S *et al* 2011 *Nat. Phys.* **7** 656–62
[11] Krüger M, Schenk M and Hommelhoff P 2011 *Nature* **475** 78–81
[12] Kling M F, von den Hoff P, Znakovskaya I and de Vivie-Riedle R 2013 *Phys. Chem. Chem. Phys.* **15** 9448–67

[13] Skruszewicz S, Tiggesbäumker J, Meiwes-Broer K H, Arbeiter M, Fennel T and Bauer D 2015 *Phys. Rev. Lett.* **115** 043001
[14] Süßmann F *et al* 2015 *Nat. Commun.* **6** 7944
[15] Seiffert L, Süßmann F, Zherebtsov S, Rupp P, Peltz C, Rühl E, Kling M F and Fennel T 2016 *Appl. Phys.* B **122** 1–9
[16] Rupp P *et al* 2017 *J. Mod. Opt.* **64** 995–1003
[17] Kumarappan V, Krishnamurthy M and Mathur D 2002 *Phys. Rev.* A **66** 033203
[18] Döppner T, Fennel T, Radcliffe P, Tiggesbäumker J and Meiwes-Broer K H 2006 *Phys. Rev.* A **73** 031202
[19] Krishnan S R *et al* 2011 *Phys. Rev. Lett.* **107** 173402
[20] Saalmann U and Rost J M 2008 *Phys. Rev. Lett.* **100** 133006
[21] Fennel T, Döppner T, Passig J, Schaal C, Tiggesbäumker J and Meiwes-Broer K H 2007 *Phys. Rev. Lett.* **98** 143401
[22] Springate E, Aseyev S A, Zamith S and Vrakking M J J 2003 *Phys. Rev.* A **68** 053201
[23] Passig J, Irsig R, Truong N X, Fennel T, Tiggesbäumker J and Meiwes-Broer K H 2012 *New J. Phys.* **14** 085020
[24] Fennel T, Bertsch G and Meiwes-Broer K H 2004 *Eur. Phys. J.* D **29** 367–78
[25] Köhn J, Redmer R and Fennel T 2012 *New J. Phys.* **14** 055011
[26] Calvayrac F, Reinhard P G, Suraud E and Ullrich C 2000 *Phys. Rep.* **337** 493–578
[27] Féret L, Suraud E, Calvayrac F and Reinhard P G 1996 *J. Phys. B: At. Mol. Opt. Phys.* **29** 4477
[28] Ullrich C A, Domps A, Calvayrac F, Suraud E and Reinhard P G 1997 *Z. Phys.* D **40** 265–70
[29] Domps A, Reinhard P G and Suraud E 1998 *Phys. Rev. Lett.* **81** 5524–7
[30] Domps A, Reinhard P G and Suraud E 2000 *Ann. Phys.* **280** 211–35
[31] Köhn J, Redmer R, Meiwes-Broer K H and Fennel T 2008 *Phys. Rev.* A **77** 033202
[32] Gunnarsson O and Lundqvist B I 1976 *Phys. Rev.* B **13** 4274–98
[33] Passig J *et al* 2017 *Nat. Commun.* in preparation